The 7th International Supercritical CO_2 Power Cycles Symposium
February 21 - 24, 2024, San Antonio, Texas
Paper # 116

The effect of elevated temperatures and pressure on five metallic materials in a quasi-static supercritical CO_2 environment

Margarita Ilinich
Research Engineer
Natural Resources Canada
Ottawa, ON

Kourosh Zanganeh
Senior Research Scientist & Group Leader
Natural Resources Canada
Ottawa, ON

Taylor Robertson
Research Officer
National Research Council of Canada
Ottawa, ON

Holly Dole
Research Scientist
Natural Resources Canada
Ottawa, ON

Dongyi Seo
Senior Research Officer
National Research Council of Canada
Ottawa, ON

Hamid Radfarnia
Research Scientist
Natural Resources Canada
Ottawa, ON

Henry Saari
Associate Professor
Carleton University
Ottawa, ON

Ashkan Beigzadeh
Research Engineer
Natural Resources Canada
Ottawa, ON

ABSTRACT

The supercritical carbon dioxide (sCO_2) Brayton power cycle is a promising alternative to steam Rankine cycle due to its higher cycle efficiency at equivalent turbine inlet conditions. It uses sCO_2 as the working fluid in a closed or semi-closed Brayton cycle. This cycle is applicable to most thermal energy sources, such as fossil fuel, nuclear, solar, geothermal, and waste heat, for power conversion and generation. Achieving the full benefits of the sCO_2 cycle depends on overcoming a number of engineering and materials science challenges that impact the technical feasibility and operability of the cycle, as well as its economic viability. While the components of this cycle can operate in a wide range of temperature, materials corrosion at the higher temperatures is more significant and requires further investigation. The work reported here focuses on the performance of metal alloys that can be used in manufacturing of high-temperature components of sCO_2 power cycles. Until recently, the performance data for materials in sCO_2 environment has been very scarce. Hence, it is required to further investigate the effects of elevated temperature and pressure on corrosion performance of metal alloys in this environment.

For this investigation, five metal alloys were chosen for testing at two temperatures (550^{o}C and 700^{o}C) and at 200 bar, in 500-hour intervals for a total of 1500 hours. The samples tested were Inconel 740H, Inconel 625, Haynes HR-120, 316L stainless steel, and GR 91 steel; GR 91 steel was only tested at 550^{o}C due to its lower temperature rating, whereas Inconel 740 H was tested only at 700^{o}C due to its high

corrosion resistance. The samples were tested in a unique corrosion test rig, jointly developed by CanmetENERGY-Ottawa and Carleton University, in a quasi-static stream with 99.8% CO_2 purity. Following the exposure at elevated temperatures, samples were weighed (to compare with base line "as-received" samples) and then the corresponding metallographic samples were characterized using optical and scanning electron microscopes (SEM) and X-ray diffractometer (XRD). It should be noted that this work was originally a part of a DOE-funded Round Robin test program; however, the testing could not be completed in time to be included in the Round Robin's final report and hence is presented here.

Preliminary results for mass change at 550^{o}C and 200 bar, show that HR-120 displayed the lowest mass change of 0.07 mg/cm^2 and GR 91 steel displayed the highest mass change of 2.22 mg/cm^2 among the samples tested; in comparison, at 700^{o}C and 200 bar, HR-120 experienced a mass gain of 0.23 mg/cm^2, while 316L stainless steel experienced the highest mass gain of 0.86 mg/cm^2. Characteristics of oxides strongly depend on the compositions of the alloy samples and test temperatures. The trends observed are consistent with other reported studies; however, individual mass gains vary for each study. Further testing should be conducted for gaining a better understanding of the long-term impact of sCO_2 on materials used in these cycles. Further studies have been planned for the prolonged exposure, 3000 hours and beyond, using the same material samples.

INTRODUCTION

The sCO_2 Brayton cycle is a promising alternative to the steam Rankine cycle due to increased cycle efficiency and lower operating costs at equivalent turbine inlet conditions. The efficiency of these cycles, achieved due to unique properties of CO_2 beyond the critical point, results in a decrease of greenhouse gas (GHG) emissions when the cycles are directly, or indirectly, coupled to fossil fuel energy conversion systems. Furthermore, the higher fluid density leads to smaller equipment sizes, hence lower capital costs and smaller plant footprint. Moreover, the transition from Rankine steam cycle to sCO_2 Brayton cycle has the potential to significantly lower plant's water demand.

In contrast to the many advantages of this technology, there remains a number of engineering and economic obstacles that need to be overcome before it can be successfully deployed. Some of these challenges include development of efficient heat exchangers and turbomachinery to minimize energy losses, and materials that can safely operate in sCO_2 environment at elevated pressures and temperatures. In general, the degradation due to corrosion, oxidation and carburization of materials in sCO_2 is insignificant at temperatures below 500°C; hence, this study focuses at temperatures greater than 550^{o}C. More specifically, this paper investigates the corrosion behavior of five metal alloy samples (Inconel 740H, Inconel 625, Haynes HR-120, 316L stainless steel, and GR 91 steel) at 550°C and 700°C, at 200 bar, in quasi-static sCO_2 stream. It should be noted that this work was originally a part of the DOE-funded Round Robin test program; however, the testing could not be completed in time to be included in the Round Robin's final report and hence is presented here.

Previous studies have been conducted on austenitic steels and Ni-based alloys in sCO_2 environment at pressures in the range of 100 – 200 bars. The outcome of these works show that pressure has minimal effect on the corrosion of materials in this environment. On the other hand, temperature can cause significant changes in corrosion rate and oxide types [1], [2], and [3]. Austenitic steels, such as 316L and GR 91 have been commercially available for decades and used in boilers and high temperature piping systems. There are several studies that explore the effect of CO_2 on these two metals at temperatures ranges between 550°C to 650°C, as outlined in [4], [5], [6], and [7]. On the other hand, Ni-based alloys

can be highly resistant to corrosion and some grades are commonly used in the chemical processing and petrochemical industries, as well as in nuclear reactors and pressure vessels or heat exchangers. To this end, Inconel 625 was tested in sCO_2 environment at temperatures of up to 650°C [5] and [8]. Furthermore, the performance of Haynes HR-120 was studied at temperatures of 350°C and 600°C [7]. Inconel 740H is a relatively new alloy that has applications in supercritical water boilers [9]. In addition, performance results recently obtained through the round robin by the participating teams are reported in [2] and [10]. Table 1, depicts the respective compositions of each material sample used in the foregoing round robin, as well as this study [10]. It is also important to note that the samples used in this round of testing were supplied by Electrical Power Research Institute (EPRI) as part of the round robin program; the samples were re-sized at CanmetENERGY-Ottawa (CE-O) for use in the existing sCO2 corrosion test rig. After adjusting the samples, they were re-polished to 600 grit in accordance with the round robin program's guideline.

Table 1: Compositions of the alloys studied in the test campaign [10].

Alloy	Fe	Cr	Ni	Co	Al	Mn	Mo	Nb	Cu	Ti	Si	V	W
Gr 91	89.27	8.23	0.13	0.018	0.010	0.45	0.93	0.063	0.091	0.003	0.279	0.196	0.141
316L	68.29	16.84	9.93	0.214	<0.002	1.58	1.98	0.009	0.492	0.010	0.360	0.079	0.065
HR120	34.48	24.94	37.44	0.248	0.069	0.80	0.47	0.561	0.065	0.015	0.483	0.036	0.078
625	3.66	21.17	61.65	0.178	0.204	0.28	8.70	3.422	0.159	0.210	0.168	0.002	0.111
740H	0.11	24.14	50.42	20.421	1.312	0.23	0.31	1.559	0.002	1.374	0.153	0.008	<0.002

Experimental Setup and Procedure

The candidate materials were tested in a unique corrosion test rig that was jointly developed by CanmetENERGY-Ottawa (CE-O) and Carleton University [11]. Figure 1 shows the corrosion test rig, and Figure 2 provides a schematic of its process flow diagram. The supply CO_2 gas comes from a bulk tank located on the facility's premises and is pneumatically boosted to the test's target pressure using a sCO_2 compatible booster pump. Target pressure is achieved by adjusting a pressure regulator downstream of the booster pump. A series of heat-traced lines are used to preheat the fluid before it enters the pressurized vessel that is, in turn, installed inside a ThermCraft three-zone tube furnace XST-6-0-36-3V; the preheating allows for better control in reaching the target temperature. The tube furnace can be set to achieve a wide range of temperatures, including 550°C and 700°C. The metal samples are held in an alumina (Al_2O_3) specimen boat at the centre of the furnace (Figure 3). The corrosion test rig has been designed to operate at maximum temperatures of 750°C at 294 bar, or 800°C at 176 bar.

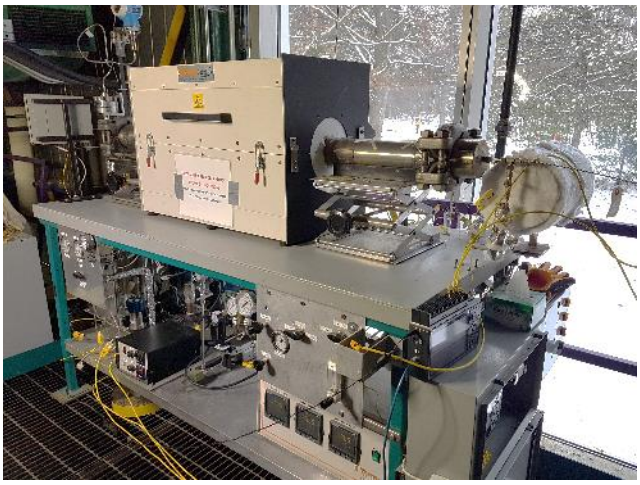

Figure 1: High pressure and temperature supercritical CO_2 corrosion test rig, jointly developed by Natural Resources Canada's CanmetENERGY-Ottawa and Carleton University.

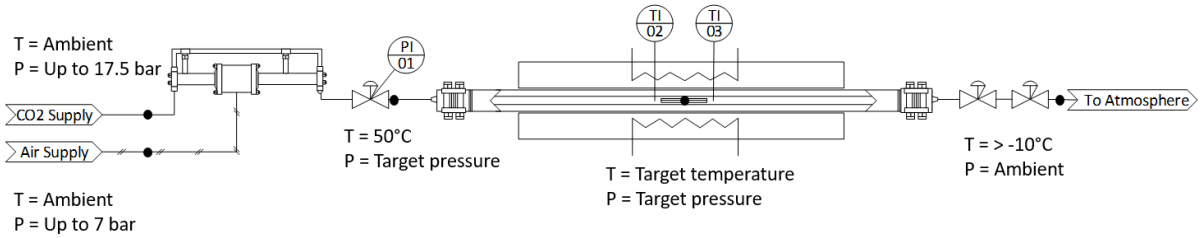

Figure 2: Schematic of the high pressure and temperature supercritical CO2 corrosion test rig's process flow diagram, jointly developed by Natural Resources Canada's CanmetENERGY-Ottawa and Carleton University.

Following the completion of sCO_2 exposure tests, the samples were naturally cooled down inside the vessel, removed from the pressure vessel, and weighed using Schuler Scientific MA-T-5 microbalance with accuracy of 1.6 μg. The as-received and post-exposure samples were characterized at National Research Council of Canada (NRC). SEM analysis was performed using Philips XL30 SFEG high-resolution scanning electron microscope using secondary electron (SE) and backscattered electron (BSE) methods. Sample preparation for cross-sectional SEM analysis included coating the samples with gold and electroplating them with copper. The samples were cold-mounted in an epoxy mixture in a vacuum chamber and sectioned using a diamond blade. Energy-dispersive X-ray spectroscopy (EDX) was utilized to identify elemental composition of phases. X-ray diffraction was applied to examine the crystallography of the samples over 2θ range of 20-90° at a scanning rate of 2.4^{o}/min. The intensity of the peaks was examined using Jade9 software, which was equipped with the International Center for Diffraction Data (ICDD) database.

Figure 3: Test samples inside the alumina specimen boat prior to the first test.

RESULTS AND DISCUSSION

Exposure to sCO_2 at 550°C and 200 bar:

Figure 4: shows the physical appearance of the four alloys studied at 550°C and 200 bar, at the beginning of testing (as received – AR), 500 hours, 1000 hours, and 1500 hours. After the first 500 hours, all samples visually maintained their polished appearances; however, GR 91 darkened slightly whereas 625 displayed a slight progression of heat-induced coloration on both faces of the samples (Figure 4q). After 1000 hours and 1500 hours, all four alloys darkened due to thickening of the oxide layers, as will be discussed in the subsequent sections; however, alloy 625 still maintained a slightly glossy appearance on the lower half of the samples.

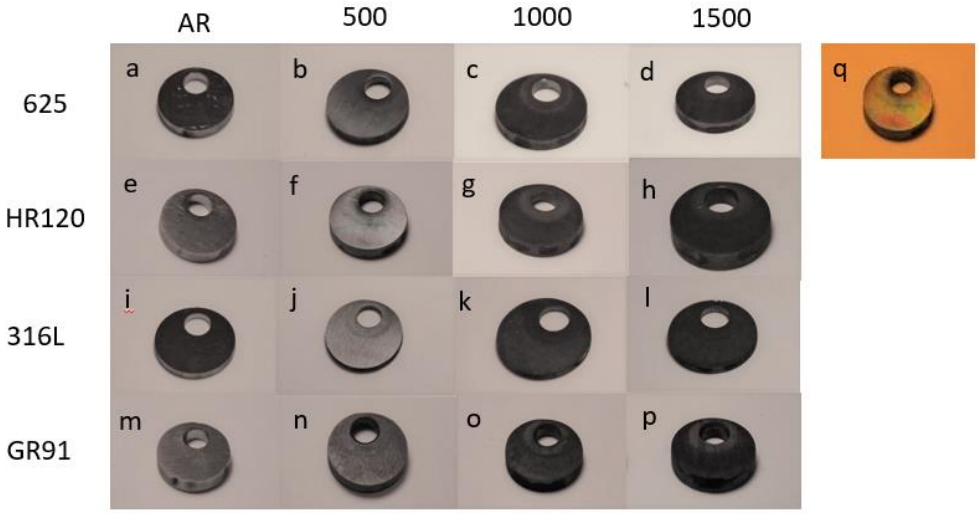

Figure 4: Visual appearance of samples exposed to 550°C at 200 bar for up to 1500 hours (a-p); (q) displays Alloy 625 after 500-hour exposure with different lighting to better capture the surface colours.

Figure 5 depicts the mass gain of the four samples examined in this study. The data obtained in this study is shown in black dashed lines (CE-O). As can be seen in this figure, GR 91 steel displayed the highest mass gain of 2.22 mg/cm^2, which is indicative of its low corrosion resistance. Although the mass gain experienced by stainless steel 316L is not as significant as for GR 91, it is still clearly outperformed by the two nickel-based alloys. Out of the four alloys exposed to these conditions, HR-120 proved to have the lowest mass gain (0.07 mg/cm^2). With the exception of GR 91 steel, the material mass gain recorded in this study appears to be slightly higher than those reported by the other groups who participated in the round robin program (KAIST, NETL, UW, and OSU) [10]. The difference could be attributed to slight differences in furnace temperature profile and pressure reached at each facility, as well as sample test apparatus, holder design, and the associated flow pattern around the samples.

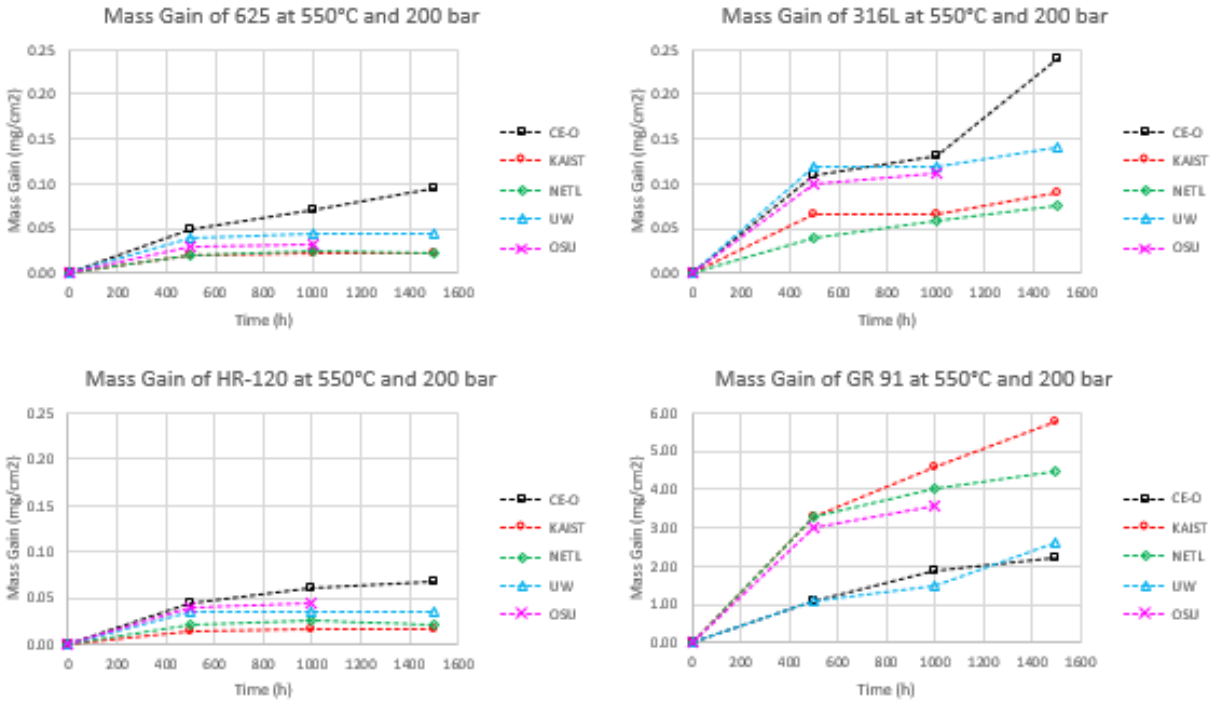

Figure 5: Mass gain of sample coupons exposed to 550°C at 200 bar compared to results obtained by other institutions [10].

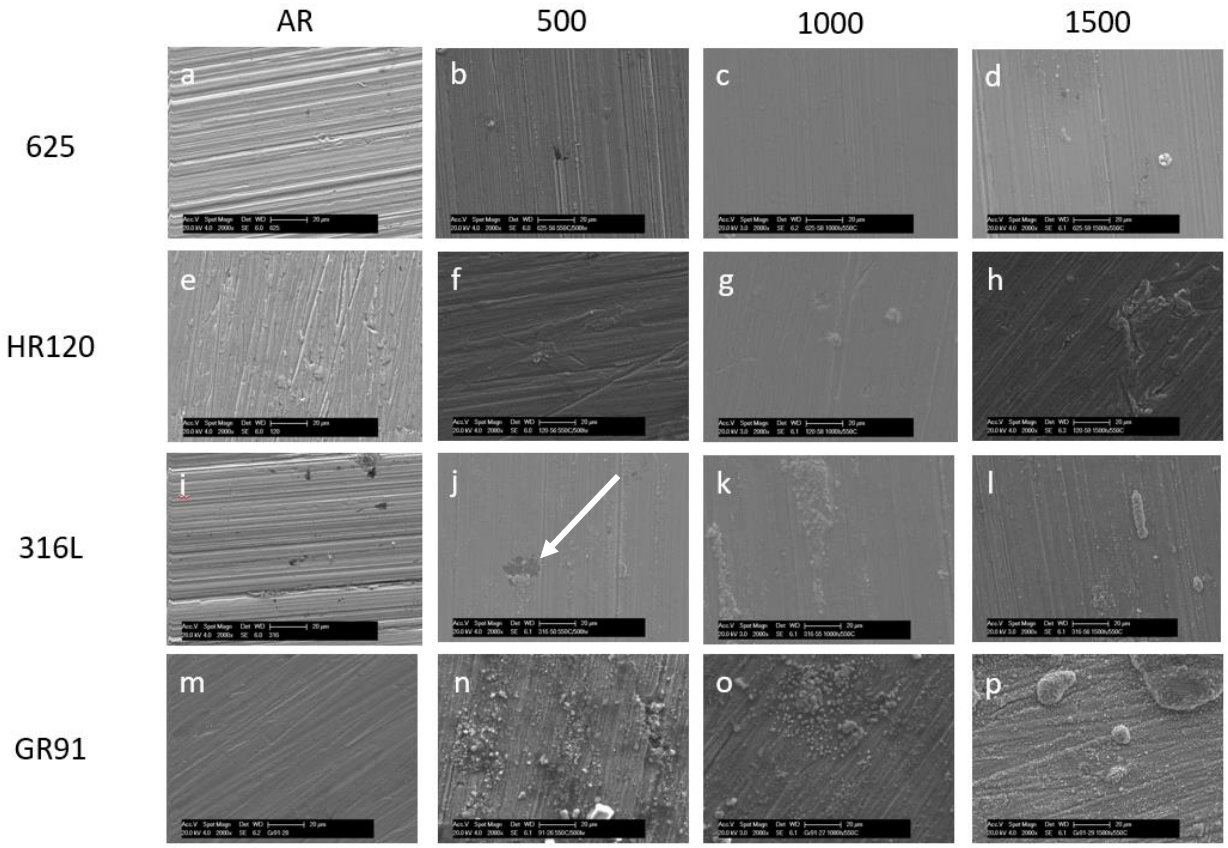

Figure 6: Surface SEM of samples at 550°C and 200 bar at 2000x magnification.

Figure 6 depicts the surface SEM images of the alloys examined in this study at 2000x magnification, for as received (AR), 500, 1000, and 1500 hours. After 500 hours, it can be seen that all alloys developed a thin base layer of oxides, as the polishing marks are still detectable on the substrate. The base layer oxide became thicker as the exposure time increased. The oversized oxide growths can be clearly seen along the surface of GR 91 steel (Figure 6n), and surrounding the large pit on the surface of 316L after 500 hours (indicated by the arrow in Figure 6j). The clusters developed in these steel samples (Figure 6 j, k, l, n, o, p) continued to grow and combine for the duration of the test runs. Additional pitting was not observed on the surface of 316L beyond 500 hours, which was attributed to an increase in the oxide layer thickness.

Some areas of greater oxide growth began to develop on the surface of HR-120 and 625 after 1000 hour and 1500 hour exposures, respectively. The elemental composition of the surface oxide layers was also determined by EDX scans (not shown here). The area scans of 316L and GR 91 revealed that the base oxide layer is composed of Fe and Cr, with Mn based spinel contents. The EDX spot scans of oversized oxide growths also showed that the area of greater oxide growth in 316L and GR 91 is mainly covered by Fe-based oxides. The area scans of HR-120 and Inconel 625 indicated that the surface oxide is comprised primarily of Cr-based oxides with some spinel contents. Therefore, it seems that the primary oxide for nickel-based alloys is likely Cr_2O_3, whereas Fe_3O_4 is likely more prominent for the two steels.

Figure 7 and Figure 8 show the cross sectional views of all samples at 500, 1000, and 1500 hour exposure intervals at both low and high magnifications. In addition, further analysis was made by EDX scans to identify the elemental composition of the oxide layers and surface of the substrate (not shown here). As can be seen from Figure 7 and Figure 8, Inconel 625 and Haynes HR-120 develop the two thinnest stable oxide layers, even after 1500 hours (Figure 8c, f).

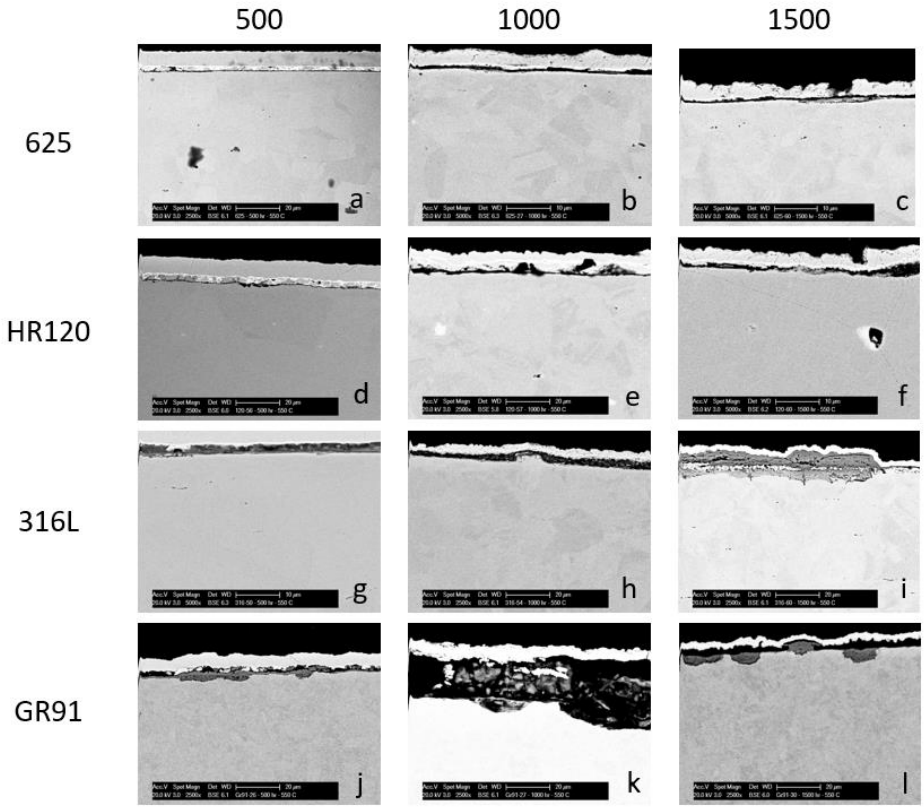

Figure 7: Cross sectional SEM of Inconel 625, Haynes HR-120, 316L stainless steel and GR91 steel samples at 550^{o}C and 200 bar at 2500x magnification, except: (b, c) 625 after 1000 hours and 1500 hours at 5000x magnification, (f) HR-120 after 1500 hours at 5000x magnification, (g) 316L after 500 hours at 5000x magnification.

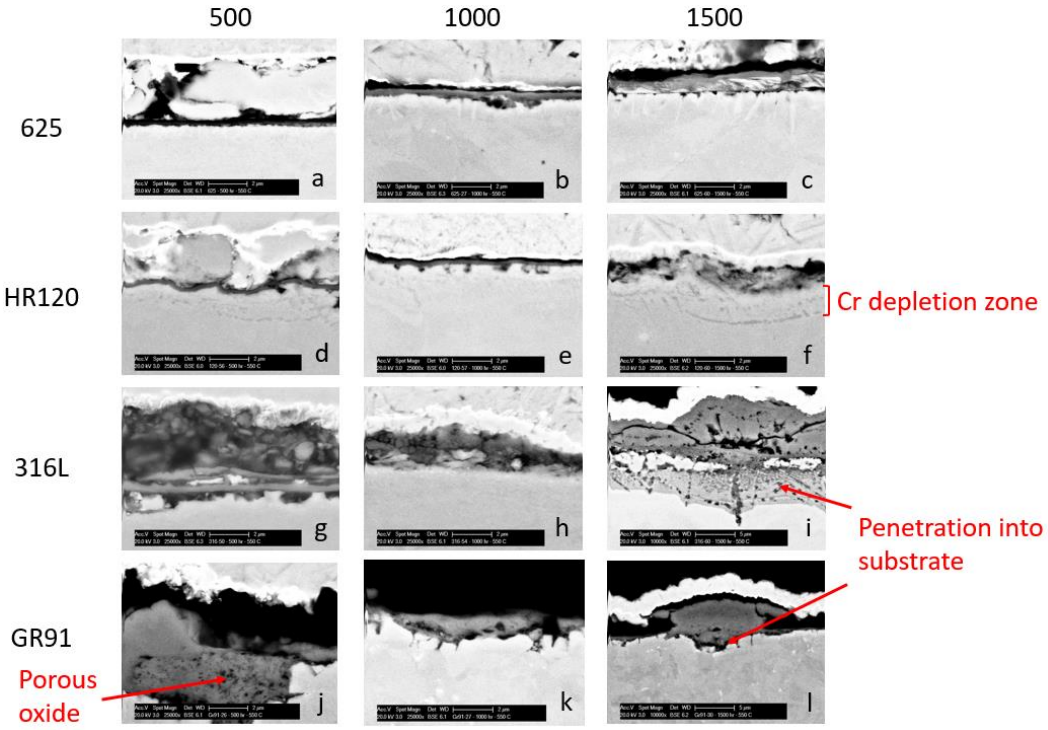

Figure 8: Cross sectional SEM of Inconel 625, Haynes HR-120, 316L stainless steel and GR91 steel samples at 550^{o}C and 200 bar for 1500 hours at 25000x magnification; 316L and GR 91 at 1500 hours are shown at 10000x magnification.

The overall thicknesses are presented in Figure 9. The oxide layer for the Ni-base alloys remains thin and gradually increases, after each exposure. However, the recorded measurements for 316L and GR 91 show loss of oxide layer after 1000 hours; this is likely due to the loss of oxide layer during preparation of samples for characterization analysis.

HR-120 maintained its protective Cr_2O_3 oxide layer up to 1500 hours of exposure, which is an indication of a fair corrosion resistance performance of this material. Cr_2O_3 is known for good corrosion protection due to good adhesion to the substrate, minimal porosity, low oxygen diffusivity, and similar relative volume compared to the substrate [12]. Some evidence of oxide penetration into the substrate (figure not shown) was also detected. A Cr-depletion zone was indicated by the formation of voids within the substrate near the surface (can be seen in Figure 8f at 1500 hours), which is a cause for concern since the oxide forming elements are progressively depleted in this zone throughout the exposure interval. The loss of Mn from the grain boundaries to form spinel oxide at the surface of the substrate is another concern. The growth of a spinel oxide other than Cr_2O_3 oxide at the surface of the substrate can be also distinguished in Figure 8f.

Inconel 625 had an overall good resistance to oxidation for an exposure duration up to 1500 hours, presenting a thinner oxide layer formation than HR-120, as can be seen in Figure 7 and Figure 8, primarily forming Cr_2O_3. The Cr-depletion zone was also much thinner than that observed in HR-120 (Figure 8a), which enables the material to be more resistant to an aggressive oxidative environment.

In comparison, the two steels (316L and GR 91) did not develop an effective protective oxide layer. Due to the nature of the formed oxidation phase, a shorter lifetime in an oxidizing atmosphere is expected. As can be seen in Figure 7 and Figure 8, particularly after 1500 hours (Figure 8i and l), the formation of area of high-oxide growth on these steels consumes the substrate considerably and hence can weaken

the material's mechanical stability. This oversized oxide region also does not uniformly extend across the entire surface, particularly for the 316L sample. The sample exhibited a duplex oxide composition, a thin layer of Cr_2O_3 with some penetration by a spinel. The secondary oxide phase is assumed to be Fe_3O_4, as evidenced by the elemental composition analysis. The Fe-based oxide is an active oxide phase, and its ability to form the spinel phase that penetrates into the thin layer of Cr-based oxide is a matter of concern for the 316L material. Therefore, with the longer exposure time, the Cr-based oxide layer becomes thinner, weakening the corrosion resistant layer of the material (in this case Cr-based oxide layer).

Grade 91 exhibited significant oxidation at exposure to sCO_2 at 550 °C. The cross sectional images in Figure 7j-l and Figure 8j-l revealed the formation of large excessive oxide growths, which penetrated into the substrate. These oversized oxides appeared to be connected by a thin layer of base oxide that narrowed with the progression of undersized growth oxide layers. As stated before, this oxidation product was primarily the active oxide phase Fe_3O_4 that led to significant depletion of the substrate. The main issue with GR 91 is the composition of the base oxide layer; this oxide contains greater Cr and Mn content than the surface oxide leading to a porous structure, which exposes the substrate to progressive oxidation.

The images for 316L and GR 91 after 1500-hour exposure were shown in Figure 8i and l at a lower magnification (10000x) to better capture the degree of oxide penetration. Furthermore, when the thickness of oxide layer was measured, two sets of measurements were required for 316L stainless steel after 1500 hours – one measurement capturing the thickness of base oxide, and another capturing the areas of excessive oxide growth. Prior to the 1500 hour analysis, there was no clear distinction between the Cr-based, Fe-based, and spinel oxides. Due to the difficulty distinguishing between the aforementioned oxide types, the thickness measurements showed a higher variation. The results shown in Figure 9 are the average of six measurements per alloy.

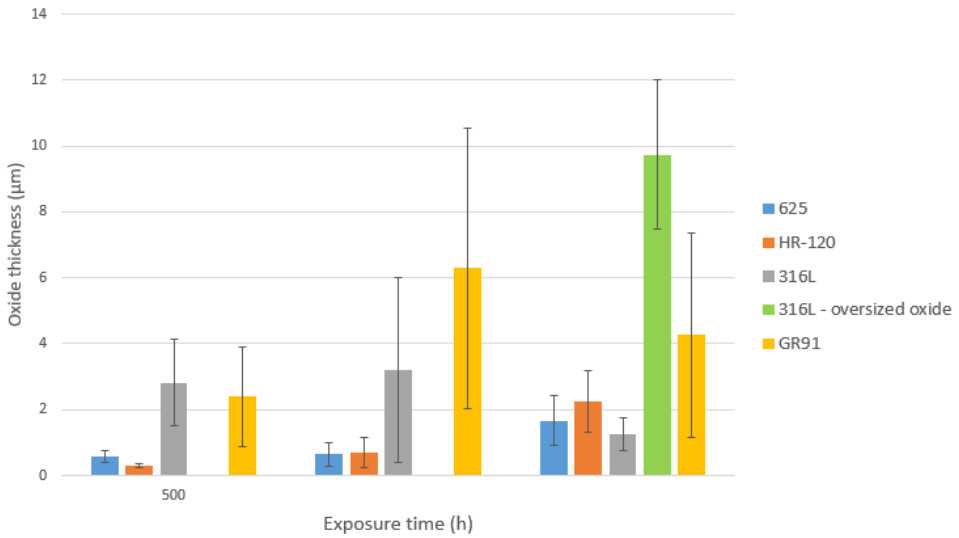

Figure 9: Oxide layer thickness of Inconel 625, Haynes HR-120, 316L stainless steel and GR91 steel exposed to sCO_2 at 550°C and 200 bar.

XRD results for the four alloys are presented in Figure 10 and Figure 11. These results confirm that the primary oxide for the two nickel alloys is Cr_2O_3, whereas Fe_3O_4 is primary oxide for the steels. Further observations indicated that the level of oxidation identified for 625 and HR-120 is relatively low, based

on the intensity peaks in Figure 10. The peaks associated with the substrate materials are significantly higher than those of the oxides. In addition to the primary oxide Cr_2O_3, Inconel 625 exhibits the formation of additional crystalline phases, including Mn, Ni and Nb substitutions in the chromia or spinel crystal structures, whereas HR-120 displays the formation of additional oxides, in the form of Mn-Fe-Cr spinel structure. It is evident that the 316L stainless has significant oxidation due to the higher intensity peaks and the number of oxide peaks. A split in the austenite peak can be seen at ~44° 2θ, which corresponds to the alteration of cell size in austenitic lattice [13]. Finally, GR 91 shows high intensity peak associated with Fe_3O_4, which is indicative of lower corrosion resistance in this type of alloy.

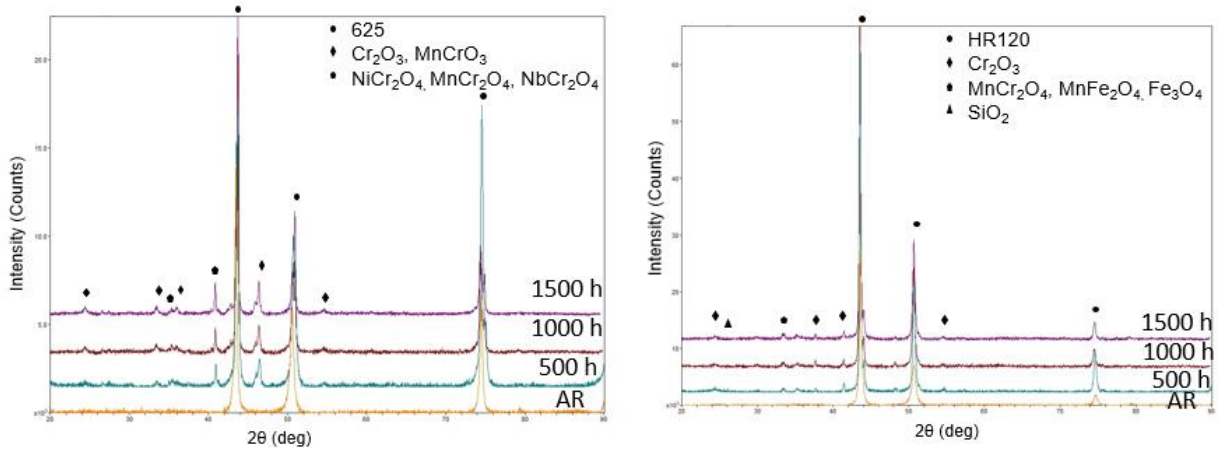

Figure 10: XRD analysis of Inconel 625 and Haynes HR-120 after exposure to sCO_2 at 550°C and 200 bar.

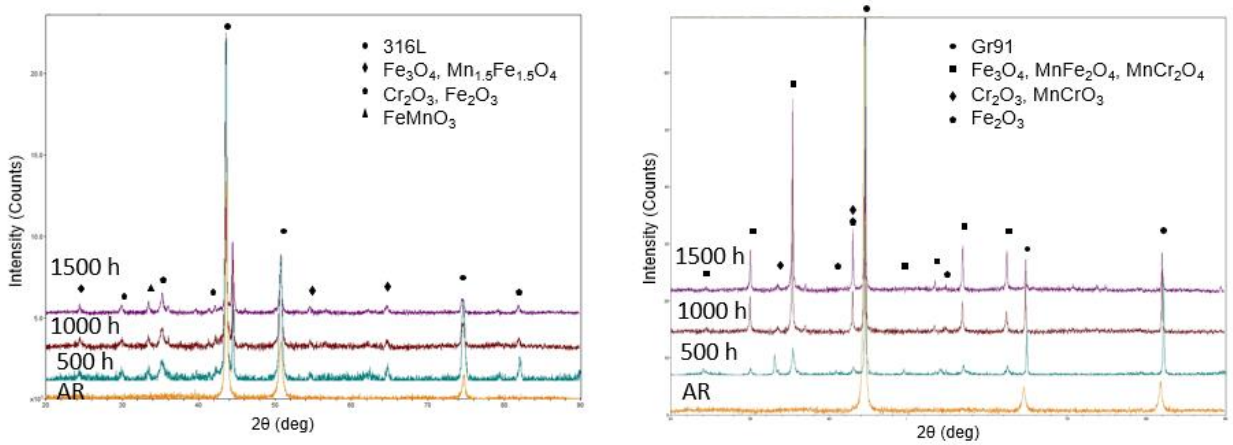

Figure 11: XRD analysis of 316L stainless steel and GR 91 steel after exposure to sCO_2 at 550°C and 200 bar.

Exposure to sCO_2 at 700°C and 200 bar:

Inconel 740H, Inconel 625, Haynes HR-120, and 316L stainless steel were studied in the second part of this test campaign. The physical appearance of the four alloys after each interval is shown in Figure 12. Unlike the 550°C study, the samples revealed clear signs of oxidation indicated by the change in color after the first 500 hours. A chip was noted on the side of HR-120 sample (Figure 12j), likely caused during machining of the sample. By the end of the 1500 hours, through visual inspection, Inconel 625 changed the least while 316L stainless steel seemed to be the most discolored, as a result of exposure to sCO_2 environment. After the 1500 hours, all samples exhibited wear in the bottom half of the sample,

which was attributed to the shape of the specimen boat at the inlet. Furthermore, the circular marks that can be seen on the 316L samples throughout the testing and on the HR-120 sample after 1500 hours are caused by the alumina spacers used to separate samples during test runs (as can be seen in Figure 3). Although alumina is an inert material, 316L experienced some minor fusion of the spacer material.

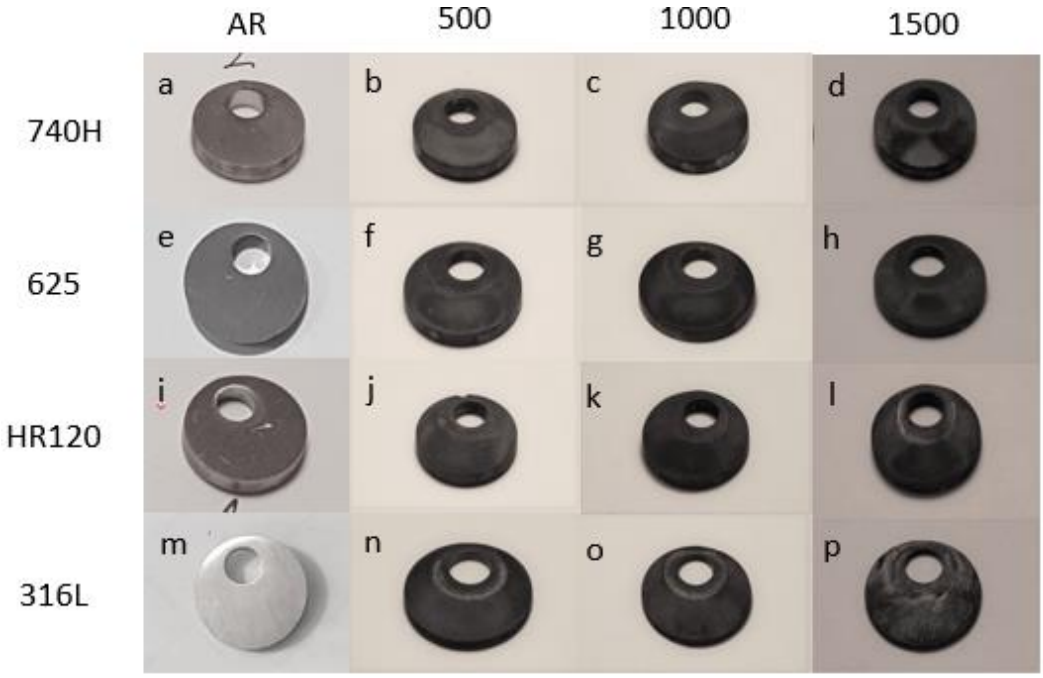

Figure 12: Visual appearance of samples exposed to 700°C at 200 bar for up to 1500 hours of exposure.

Figure 13 depicts the mass gain experienced by the tested alloys. The results obtained through this study are plotted in black dashed lines (CE-O). The 316L stainless steel presented the highest mass gain of 0.88 mg/cm^2. The three Ni-base alloys all displayed a similar mass gain between 0.23 and 0.28 mg/cm^2, with the lowest mass gain experienced by HR-120 (0.233 mg/cm^2), closely followed by 625 (0.235 mg/cm^2). The trends observed are consistent with the results reported by others participants of the round robin test campaign [10]. The lower mass gain observed for 316L after 1500 hours, in comparison to the results obtained at UW, is likely due to spallation of some oxides during the final exposure (based on the physical appearance of the sample).

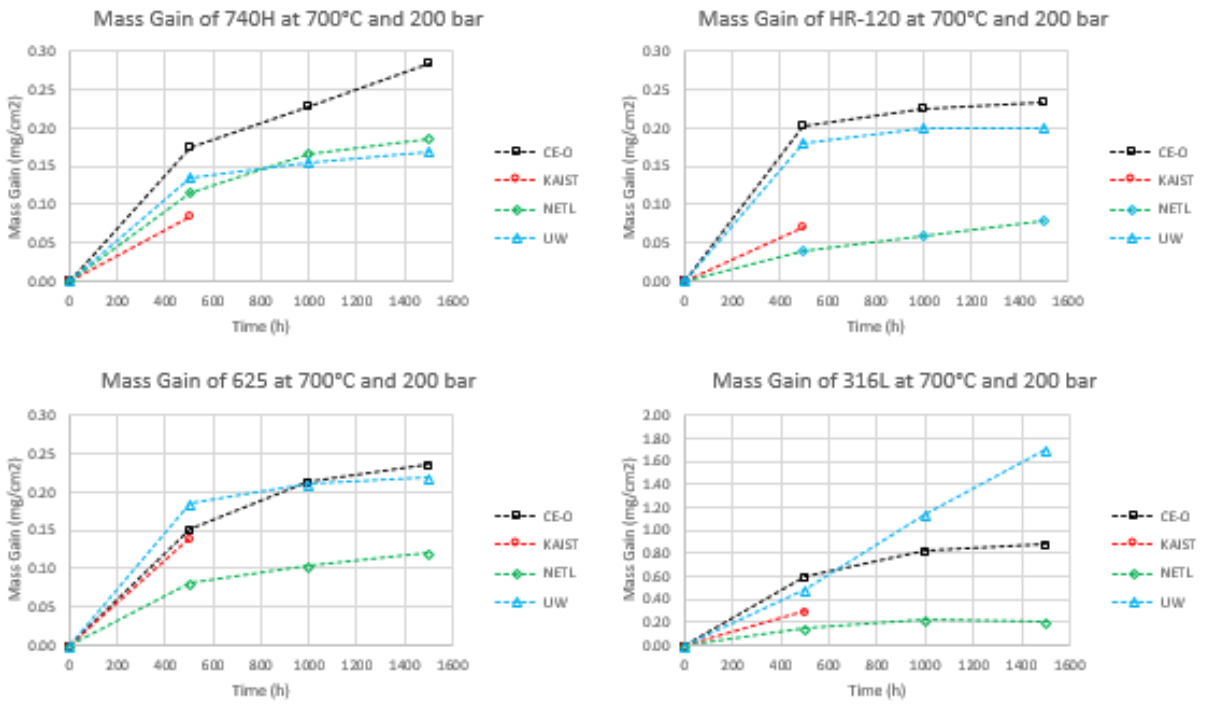

Figure 13: Mass gain of sample coupons exposed to sCO_2 at 700°C at 200 bar compared to results obtained by other institutions [10]

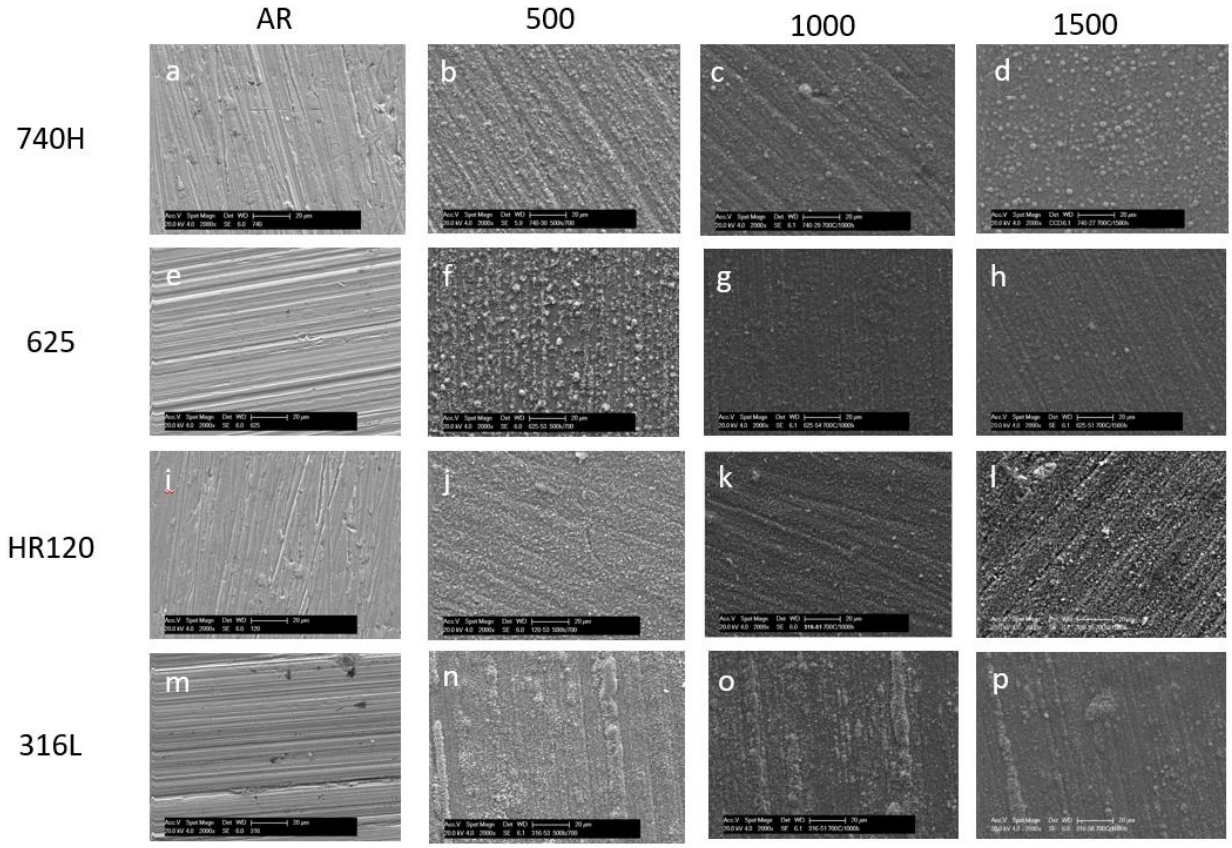

Figure 14: Surface SEM of samples at 700°C and 200 bar at 2000x magnification.

Figure 14 shows the surface SEM images of Inconel 740H, Inconel 625, Haynes HR-120, and 316L stainless steel before the exposure (as received-AR), as well as after 500, 1000, and 1500 hours. Although polish marks were still visible on the surface of each alloy, a substantial layer of oxide was detected after the first time interval. The SEM analysis of 316L stainless steel showed that the morphology of the sample surface was composed of a fairly uniform base oxide layer with rows of excess oxide growths in the direction of polish marks (Figure 14n-p). Haynes HR-120 exhibited a consistently uniform base oxide layer throughout the exposure; the substrate was fully covered by the oxide layer even after the first 500 hours (Figure 14j). Post-exposure SEM analysis identified that Inconel 625 exhibited limited oxide growth after 500 hours (Figure 14f), but experienced a full coverage of the substrate by a base oxide layer at 1000 hours onwards (Figure 14g, h). Inconel 740H developed a thin base layer after 500 hours, which is indicated by high visibility of the polish marks (Figure 14b). After 1000-hour exposure, small grains (less than 5 μm) formed on the surface of the substrate as can be seen in Figure 14d.

By studying the EDX scans (not shown here), it was established that the three nickel-based alloys exhibit a Cr-based oxide as the base layer, likely Cr_2O_3 as seen during the 550°C tests. Alloy 625 additionally displayed evidence of Nb-rich oxides at the interface of the oxide layer with the substrate. 740H displayed an increased content of Nb within the greater oxide growths. The area scans (not shown here) for HR-120 indicate that the surface oxides are primarily Cr-based with high content of Mn spinels. 316L exhibited a Cr-based oxide layer with a Fe-based oversized oxide growths.

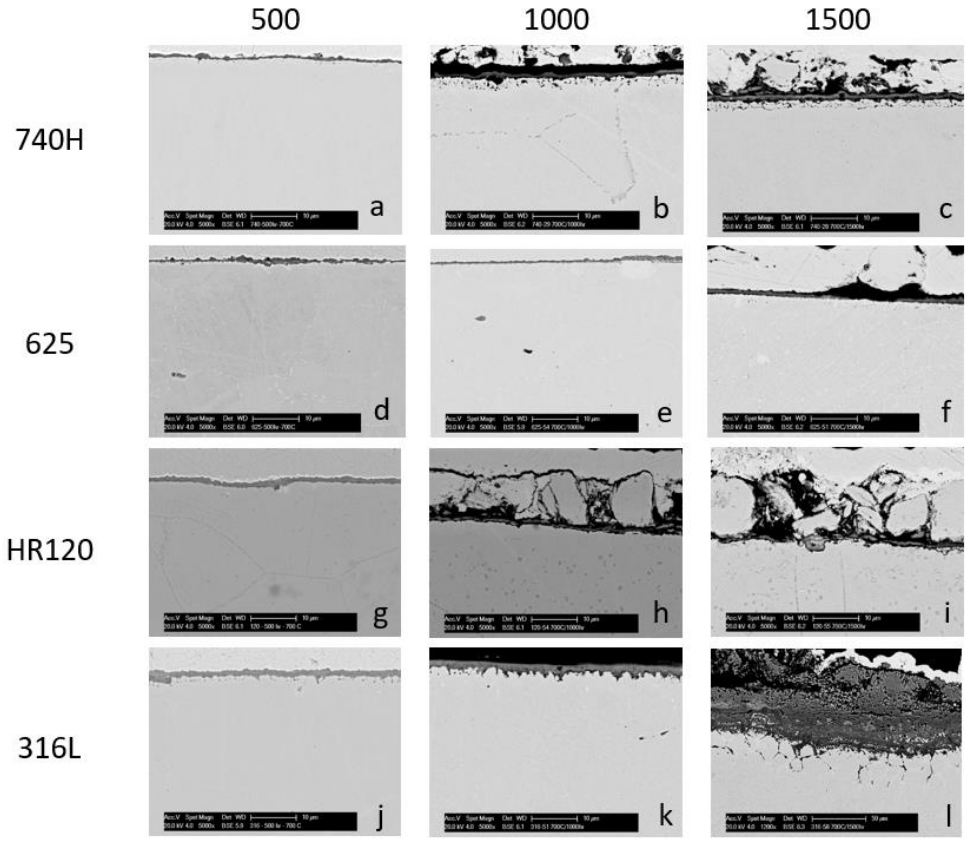

Figure 15: Cross sectional SEM of samples at 700°C and 200 bar for up to 1500 hours at 5000x magnification except (l) 316L after 1500 hours is shown at 1200x magnification.

Figure 15 and Figure 16 show the cross section SEM images of the samples at low (5000x, except Figure

15l is 1200x) and high (20000x) magnifications. Characterization of the samples proved to be non-trivial as it was challenging to maintain the Cu/Au coating adhered to the oxide layer on many of the samples during processing, especially after the 1500-hour exposure. Due to this ongoing issue, in some cases, in addition to the oxide layer, epoxy captured particulates of Cu, substrate and polishing media as can be seen in in Figure 15b, c, h, i and Figure 16b, c, h, i. The lower magnification is shown to better convey the degree of oxidation of 316L stainless steel. In the case of 316L, a duplex oxide layer was observed, with a uniform base layer of Cr_2O_3 accompanied with oversized areas of Fe_3O_4 above this base layer, where the latter one could penetrate into the substrate by the extension of exposure time. This is indicative of low operational life expectancy of 316L in the presence of an oxidizing environment due to the gradual loss of material integrity.

The oxide layer of HR-120 maintained a bi-layer structure: discontinuous base layer and a more uniform upper layer. This material displayed a considerable amount of active corrosion near grain boundaries and oxide penetration at extended time intervals, as can be seen in Figure 15i and Figure 16i at 1500 hours. Furthermore, HR-120 displayed the thickest Cr-depletion zone between all alloys, especially after 500 hours of exposure (Figure 16g).

Alloy 740H displayed a uniform, thin layer of oxidation; however, depletion of oxide-forming elements from the surface of the substrate and from the grain boundaries was noted. Inconel 625 exhibited the thinnest oxide layer, similar to the 550°C results. The average thickness of oxide product layers obtained from the cross sectional SEM images is provided in Figure 17. As can be seen in the figure, two oxide measurements were performed for 316L – one of the base oxide layers composed primarily of Cr-based oxides, and another for Fe-based oversized oxides. The results shown are the average of six measurements. In general, as expected, the longer exposure time resulted in larger oxide layer thickness. However, errors arise due to loss of parts of oxide layer during preparation of samples for cross sectional SEM analysis. This can justify the decrease in the observed oxide layer thickness with the increase in exposure time.

Inconel 740H and the runaway Fe-based oxides detected on 316L stainless steel followed a stepwise increase in the oxide layer. The other alloys displayed a decrease in the oxide product between 1000 and 1500 hours, which is likely a result of the loss of oxide during the sample preparation for the SEM characterization. As a result, based on the characterization analysis and limited exposure time of 1500 hours, 625 is deemed to be the most favourable alloy at the test condition of 700°C, displaying a thin and stable oxide layer despite the apparent loss of oxides during cross sectioning.

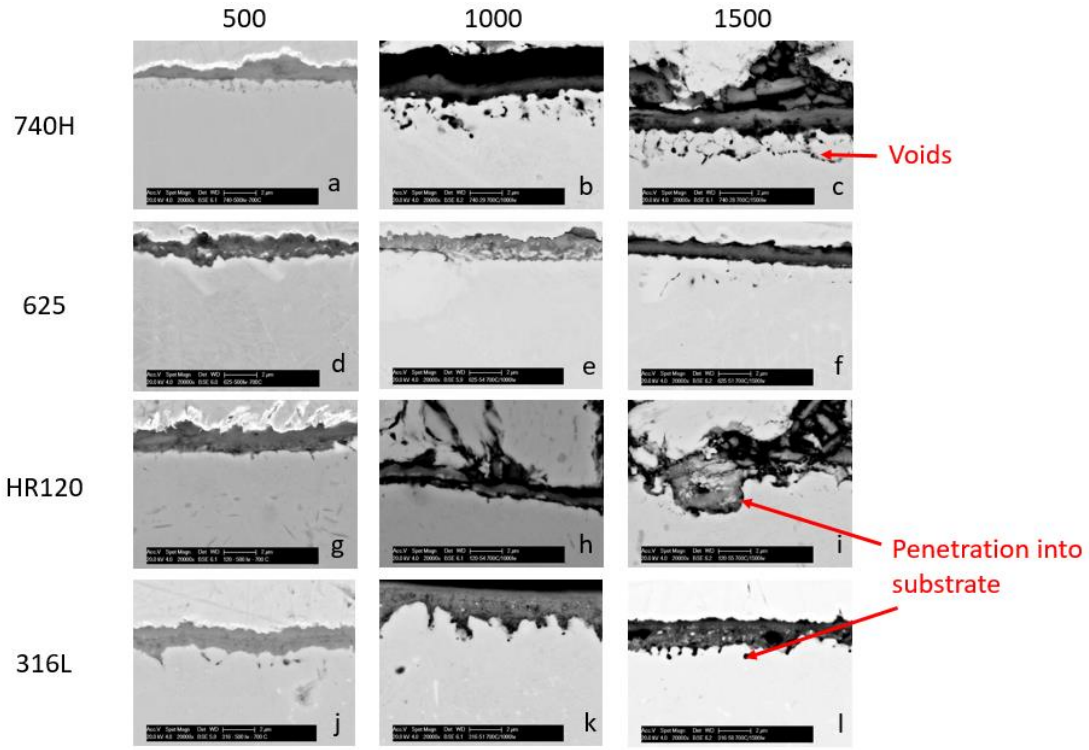

Figure 16: Cross sectional SEM of samples at 700°C and 200 bar for up to 1500 hours at 20 000x magnification.

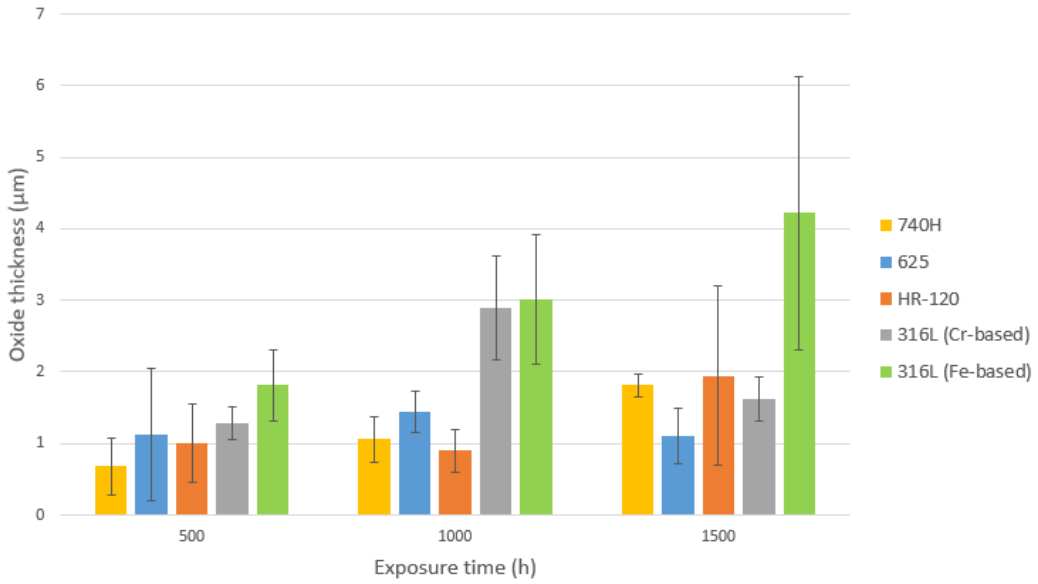

Figure 17: Oxide layer thickness of samples exposed to sCO_2 at 700°C and 200 bar.

Figure 18 and Figure 19 present the XRD results for the samples. The primary oxide for all three nickel alloys was Cr_2O_3, while for 316L, the primary oxides were both Cr_2O_3 and Fe_3O_4, as well as Fe_2O_3, and $MnFe_2O_4$ spinel. The splitting of the austenite peak at ~44° 2θ was also observed, similar to the observations reported at 550°C. Examination of HR-120 detected Cr and Mn oxides (Cr_2O_3 and spinel $MnCr_2O_3$) as the predominant crystalline phases. Presence of some SiO_2 crystalline phase was also detected during XRD analysis for HR-120 and 316L, which could be a result of the sample preparation agents. Cr_2O_3 made up the majority of the oxide on Inconel 625 throughout the test campaign with

some Mn, Ni, and Nb substitutions in the chromia or spinel crystal structures. The peak intensity of $Ni_3(Mo, Nb)$ crystal phase, formed on the surface of substrate, was noted to reduce over the course of exposure. Finally, 740H also displayed Cr_2O_3 as the primary oxide with a minor phase of spinel such as $NiCr_2O_4$. One feature of 740H, which was not detected in the other alloys, was the formation of an Al_2O_3 layer at the surface of the substrate, as detected in the XRD pattern (Figure 18). The formation of a protective Al_2O_3 oxide is desired particularly in gas turbine applications as it forms a barrier to oxygen ion diffusion [14]. However, in this study 740H displayed many voids along the grain boundaries and a fairly sizable Cr-depletion zone, which is indicative of metallic ion migration to the oxide layer.

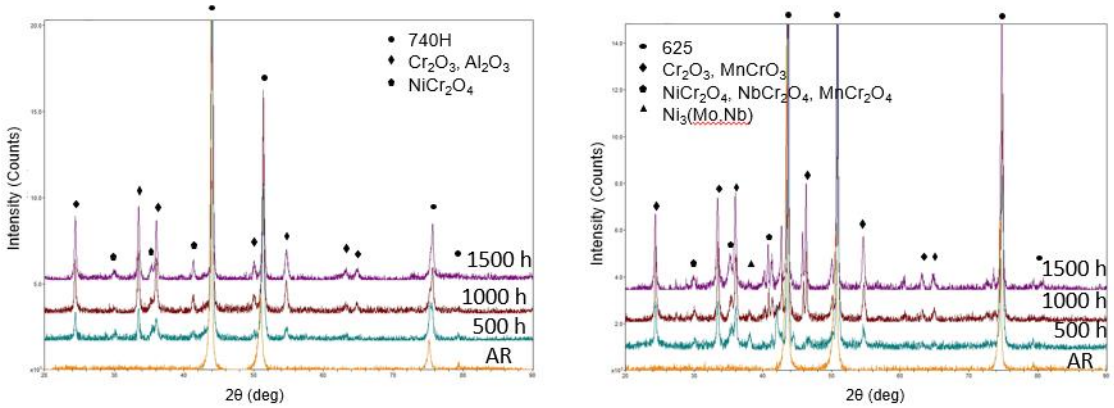

Figure 18: XRD analysis of Inconel 740H and Inconel 625 after exposure to sCO_2 at 700°C and 200 bar.

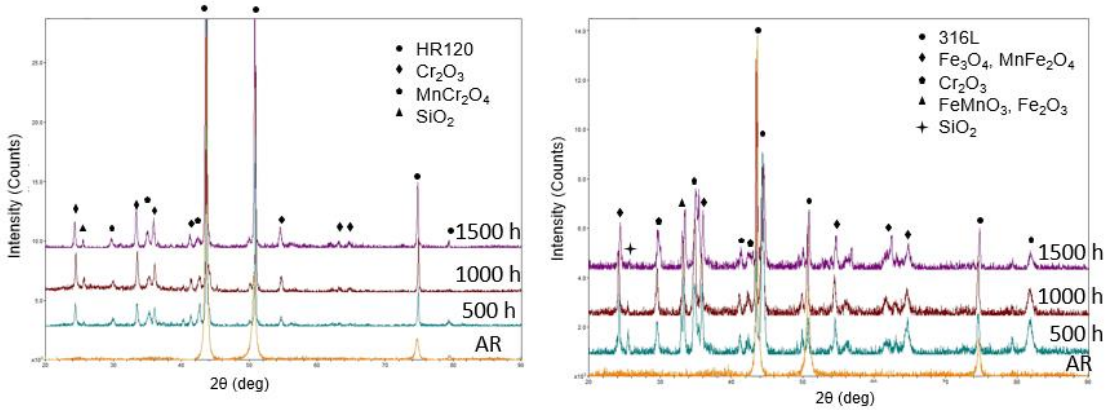

Figure 19: XRD analysis of Haynes HR-120 and 316L stainless steel after exposure to sCO_2 at 700°C and 200 bar.

Comparing the mass gain and oxide product thickness of Inconel 625, Haynes HR-120, and 316L stainless steel, it was noted that the mass gain of these alloys after 500 hours exposure to sCO_2 at 700°C at 200 bar was significantly higher than those of 550°C exposure. 316L gained about 5.6 times more mass at 700°C compared to 550°C, whereas HR-120 and 625 gained 4.6 and 3.0 times more, respectively. After 1500 hours, this mass gain ratio significantly decreased to approximately 3.5-2.5 times, 316L having the highest ratio and 625 the lowest. Comparing the formed oxide layer thicknesses was more challenging due to the issues with surface coating during the sample preparation for characterization purposes. As a result, 316L exhibited a significant loss of oxides at both exposure conditions and therefore, only 625 and HR-120 can be compared objectively. As expected, both nickel-based alloys developed thicker oxide layers during the 700°C runs; the difference was about 1.9 times for 625 and 3.5 times for HR-120 compared to the 550°C results. Similar to the mass gain trends, the difference between the thicknesses of the oxide layers, at the two temperatures under study, decreased with increasing exposure time. By the end of the test run at 1500 hours, the thickness of the oxide layer of HR-120 at 700°C was 0.86 times

of what resulted at 550°C, while this difference was 0.66 times for Inconel 625. Overall, Inconel 625 revealed the best performance at both exposure temperatures as it exhibited the most protective oxide layer and one of the thinnest oxide layers. For operations at temperature up to 550°C, HR-120 could also be a reasonable option; however, 316L and GR 91 are not recommended. Similarly, at 700°C, Inconel 740H would also make a reasonable choice, but the higher cost may be of consideration.

Conclusion:

In this study, five metal alloys were exposed to sCO_2 environment at elevated temperatures and pressure. Inconel 625, Haynes HR-120 and 316L stainless steel were studied at 550°C and 700°C, at 200 bar. Additionally, Inconel 740H was examined at 700°C, and GR 91 steel was only studied at the lower temperature of 550°C, due to its low corrosion resistance at elevated temperatures. The materials were exposed to high purity sCO_2 for durations of 500 hours, 1000 hours, and 1500 hours. After each interval, a sample of each individual alloy was removed from vessel for mass gain measurements and characterization analysis using SEM, EDX and XRD techniques. The results obtained from this study showed that Inconel 625 was the best oxidation-resisting alloy, resulting in the thinnest protective oxide layer for both conditions. The primary oxide formed on the surface of this alloy for both tests was Cr_2O_3, a passive oxide with minimal porosity, low oxygen diffusivity, and good adhesion to the substrate. Alloy 740H also performed well when exposed to 700°C; showing a resulting primary oxide layer of Cr_2O_3 with an Al_2O_3 diffusion layer that was formed at the substrate surface; however, it is possible that that Al_2O_3 layer may not be as beneficial as first thought.

Haynes HR-120 exhibited satisfactory corrosion resistance at 550°C, where Cr_2O_3 was the main component of the oxide layer. At the substrate surface, the Cr-based top layer was accompanied by a thin bottom layer of Mn based spinel/SiO_2. Some evidence of oxide penetration into the substrate was also observed, which became much more severe at exposure to 700°C. The primary concern with HR-120, particularly at high temperatures such as 700°C, is the progressive penetration of oxide species into the substrate that can lead to active corrosion and eventually material failure. The Fe-based alloys, GR 91 and 316L, exhibited the least corrosion resistant behavior when exposed to sCO_2 the elevated temperatures (550° and 700°C for 316L and 550°C for GR 91). The characterization of these two alloys revealed the formation of a primarily Fe_3O_4 oxide layer (an active oxidation phase) followed by a thin layer of Cr_2O_3 oxide underneath, which led to significant runaway oxidation at prolonged exposure times. Upon analysis of 316L, it was evident that the Cr_2O_3 oxide layer contained a spinel phase, and that Fe_3O_4 phase could penetrate through the Cr_2O_3 phase into the substrate leading to runaway oxidation growth and loss of integrity of the material. GR 91 steel was severely defected by the oxidation even at 550°C, forming a thick layer of oxidation products, primarily the Fe_3O_4 phase. It was also observed that the base-layer of the active Fe phase (Fe-Cr-Mn spinel phase) penetrated into the substrate and formed a porous layer, which enabled further oxidation damage to the substrate.

In conclusion, further studies are recommended in order to increase the understanding of the long-term effect of exposure of the materials under study to sCO_2 at elevated temperatures. In addition, it is worth investigating the effects of combustion impurities on the material behavior at operation conditions of pressurized oxy-combustion systems associated with sCO_2 power cycles.

REFERENCES

[1] B. Pint and J. Keiser, "Initial Assessment of Ni-Base Alloy Performance," *The Minerals, Metals & Materials Society,* vol. 67, no. 11, pp. 2615-2620, 2015.

[2] R. Oleksak, J. Tylczak, C. Carney, G. Holcomb and O. Dogan, "High-Temperature Oxidation of Commercial Alloys," *The Minerals, Metals & Materials Society,* vol. 70, no. 8, pp. 1527-1534, 2018.

[3] H. J. Lee, G. O. Subramanian, S. H. Kim and C. Jang, "Effect of pressure on the corrosion and carburization behavior ofchromia-forming heat-resistant alloys in high-temperature carbondioxide environments," *Corrosion Science,* no. 111, pp. 649-658, 2016.

[4] G. Cao, V. Firouzdor, K. Sridharan, M. Anderson and T. Allen, "Corrosion of austenitic alloys in high temperature supercritical carbon dioxide," *Corrosion Science,* vol. 60, pp. 246-255, 2012.

[5] D. Fleming and A. Kruizenga, "Identified Corrosion and Erosion Mechanisms in SCO2 Brayton Cycles," Sandia National Laboratories, Albuquerque, 2014.

[6] F. Rouillard, F. Charton and G. Moine, "Corrosion Behavior of Different Metallic Materials in Supercritical Carbon Dioxide at 550°C and 250 bars," *Corrosion,* vol. 67, no. 9, pp. 1-7, 2011.

[7] M. Walker and E. Withey, "Influence of CO2 Purity on the Corrosion of Structural Alloys for Supercritical CO2 Power Cycles," in *The 6th International Supercritical CO2 Power Cycles Symposium*, Pittsburgh, 2018.

[8] V. Firouzdor, K. Sridharan, G. Cao, M. Anderson and T. R. Allen, "Corrosion of a stainless steel and nickel-based alloys in high temperature," *Corrosion Science,* no. 69, pp. 281-291, 2013.

[9] A. Zielinski, M. Sroka and T. Dudziak, "Microstructure and Mechanical Properties of Inconel 740H after Long-Term Service," *Materials,* vol. 11, no. 2130, 2018.

[10] J. D. Tucker, B. Adam, M. Anderson, B. Pint, G. Holcomb, C. Carney, H. Saari, L. Teeter, J. Mahaffey, O. Dogan, C. Jang and S. Kung, "Supercritical CO2 Round Robin Test Program," Pittsburgh, 2018.

[11] R. G. Petrusenko, "The Development of a High Temperature, Supercritical Carbon Dioxide Corrosion Test Rig," Carleton University, Ottawa, 2011.

[12] M. Elbakhshwan, S. Gill, A. Rumaiz, J. Bai, S. Ghose, R. Rebak and L. Ecker, "High-temperature oxidation of advanced FeCrNi alloy in steam enviornments," *Journal Applied Surface Science,* vol. 426, pp. 562-571, 2017.

[13] G. Costa, N. Jacobson, D. Lukco, G. Hunter, L. Nakley, B. Radoman-Shaw and R. Harvey, "Oxidation behavior of stainless steels 304 and 316 under the Venus atmospheric surface conditions," *Corrosion Science,* vol. 132, pp. 260-271, 2018.

[14] H. Jiang, J. Dong, M. Zhang, L. Cheng and Z. Yao, "Oxidation Behavior and Mechanism of Inconel 740H Alloy for Advanced Ultra-supercritical Power Plants Between 1050 and 1170 °C," *Oxidation of Metals,* vol. 84, no. 1-2, pp. 61-72, 2015.

[15] P. Roberge, Handbook of Corrosion Engineering, New York: Mc Graw Hill, 2000.

[16] T. Shrestha, M. Basirat, I. Charit, G. Potirniche and K. Rink, "Creep rupture behavior of Grade91 steel," *Materials Science&Engineering,* no. 565, pp. 382-391, 2013.

[17] Y. H. He, L. J. Chen, R. L. McDaniels, C. R. Brooks, R. R. Seeley and D. L. Klarstorm, "Low-cycle fatigue behavior of HAYNES HR-120 alloy," *International Journal of Fatigue,* no. 24, pp. 931-942, 2002.

ACKNOWLEDGEMENTS

This research work was funded by NRCan's Program of Energy Research and Development (PERD). Alloys samples were supplied by EPRI, through Carleton University. Materials testing was performed by CanmetENERGY-Ottawa. Characterization of samples was done by National Research Council (NRC).